

(8, 22). Krill distributions are, however, notoriously patchy (23), and point estimates of abundance are unlikely to be representative of the regional mean. Previous studies comparing krill densities in open and ice-covered waters based on extrapolations from point samples reach contrary conclusions, highlighting shortcomings of these approaches. Netting surveys have suggested both that krill density is elevated under sea ice compared with that in open water (10) and that there is no difference in density (24). Spot acoustic observations in the same area found highest krill densities in open water most distant from the sea-ice edge (8). Ship-based continuous line-transect acoustic surveys have been used to estimate krill density in open water north of the sea-ice edge. A survey in the Weddell Sea (9) found a mean krill density near the ice edge of 23.2 g m⁻², which is similar to that detected in open water here. Echosounders on ice-strengthened research vessels have detected krill swarms along transects through ice-covered seas, but it has not been possible to determine krill density accurately from data collected from ships moving through ice because of interference caused by ice-breaking noise (25). The unique sampling capabilities of *Autosub-2* and echosounder combined have enabled us to describe a link between krill density and sea-ice cover directly and quantitatively.

Our data suggest krill are coupled tightly to a zone just inside the sea-ice edge. This coupling may be an example of risk balancing (1,

24), with krill locating actively at a compromise point that is both near to high concentrations of food (the ice edge) and that provides refuge from predators (air breathers that cannot dive through ice). Whatever the cause, the fact that krill do not appear to be distributed evenly under ice may mean that any reductions in ice area, perhaps following climate change (26), do not lead to directly proportional reductions in krill biomass. Any krill reductions may instead be in proportion to the reduction of ice-edge length. The purported 25% reduction in ice area in the 1960s (27) equates to a 9% reduction in edge length: consequences for krill may not have been as grave as has been implied.

References and Notes

1. L. B. Quetin, R. M. Ross, T. K. Frazer, K. L. Haberman, *Antarct. Res. Ser.* **70**, 357 (1996).
2. V. Loeb *et al.*, *Nature* **387**, 897 (1997).
3. K. Reid, J. P. Croxall, *Proc. R. Soc. London B Biol. Sci.* **268**, 377 (2001).
4. I. Everson, G. Parkes, K.-H. Kock, I. L. Boyd, *J. Appl. Ecol.* **36**, 591 (1999).
5. K. R. Arrigo, D. Worthen, A. Schnell, M. P. Lizotte, *J. Geophys. Res.* **103**, 15587 (1998).
6. T. Ichii, *Proc. National Institute for Polar Research (NIPR) Symp. Polar Biol.* **3**, 36 (1990).
7. J. W. S. Marr, *Discovery Rep.* **32**, 33 (1962).
8. K. L. Daly, M. C. Macaulay, *Deep-Sea Res. I* **35**, 21 (1988).
9. M. Godlewski, *Polar Biol.* **13**, 507 (1993).
10. V. Siegel, A. Skibowski, U. Harm, *Polar Biol.* **12**, 15 (1992).
11. I. Sprong, P. H. Schalk, *Polar Biol.* **12**, 261 (1992).
12. N. W. Millard *et al.*, *J. Soc. Underwater Technol.* **23**, 7 (1998).
13. Details of survey design, acoustic methods, and data

analysis are available on Science Online at www.sciencemag.org/cgi/content/full/295/5561/1890/DC1

14. P. G. Fernandes, A. S. Brierley, "Using an autonomous underwater vehicle as a platform for mesoscale acoustic sampling in marine environments," *ICES CM 1999/M:01* [International Council for the Explorations of the Sea (ICES), Copenhagen, 1999].
15. D. E. McGehee, R. L. O'Driscoll, L. V. Martin Traykovski, *Deep-Sea Res. II* **45**, 1273 (1998).
16. A. S. Brierley *et al.*, *Fisheries Res.*, in press.
17. J. L. Watkins, A. S. Brierley, *WG-EMM-97/46* [Commission for the Conservation of Antarctic Marine Living Resources (CCAMLR), Hobart, 1997].
18. A. S. Brierley, J. L. Watkins, C. Goss, M. T. Wilkinson, I. Everson, *CCAMLR Sci.* **6**, 47 (1999).
19. E. Ona, R. B. Mitson, *ICES J. Mar. Sci.* **53**, 677 (1996).
20. A. P. Worby, *Observing Antarctic Sea Ice* (ASPeCt, Hobart, CD-ROM, 1999).
21. D. R. Turner, N. J. P. Owens, *Deep-Sea Res. II* **42**, 907 (1995).
22. V. Siegel, B. Bergström, J.-O. Strömberg, P. H. Schalk, *Polar Biol.* **10**, 549 (1990).
23. A. W. A. Murray, *ICES J. Mar. Sci.* **53**, 415 (1996).
24. K. L. Daly, M. C. Macaulay, *Mar. Ecol. Prog. Ser.* **79**, 37 (1991).
25. A. S. Brierley, J. L. Watkins, *Can. J. Fish. Aquat. Sci.* **57** (suppl. 3), 24 (2000).
26. D. G. Vaughan, G. J. Marshall, W. M. Connolley, J. C. King, R. Mulvaney, *Science* **293**, 1777 (2001).
27. W. K. de la Mare, *Nature* **389**, 57 (1997).
28. We thank Captain Elliot, officers and crew of RRS *James Clark Ross* cruise 58, and C. Drew, P. Lens, M. Preston, M. Robjant, and R. Woodd-Walker for assistance at sea. We are grateful to D. Demer for advice on echosounder configuration, D. McGehee for target strength information, E. Murphy for comments on our draft manuscript, and A. Shanks for statistical advice. This research was funded by the UK Natural Environment Research Council.

30 November 2001; accepted 30 January 2002

The Role of Endosymbiotic *Wolbachia* Bacteria in the Pathogenesis of River Blindness

Amélie v. Saint André,¹ Nathan M. Blackwell,^{1,2} Laurie R. Hall,¹ Achim Hoerauf,³ Norbert W. Brattig,³ Lars Volkmann,³ Mark J. Taylor,⁴ Louise Ford,⁴ Amy G. Hise,¹ Jonathan H. Lass,² Eugenia Diaconu,² Eric Pearlman^{1,2*}

Parasitic filarial nematodes infect more than 200 million individuals worldwide, causing debilitating inflammatory diseases such as river blindness and lymphatic filariasis. Using a murine model for river blindness in which soluble extracts of filarial nematodes were injected into the corneal stroma, we demonstrated that the predominant inflammatory response in the cornea was due to species of endosymbiotic *Wolbachia* bacteria. In addition, the inflammatory response induced by these bacteria was dependent on expression of functional Toll-like receptor 4 (TLR4) on host cells.

Wolbachia bacteria are essential symbionts of the major pathogenic filarial nematode parasites of humans, including *Brugia malayi* and *Wuchereria bancrofti*, which cause lymphatic filariasis, and *Onchocerca volvulus*, which causes river blindness (1). *Wolbachia* spp. are abundant in all developmental stages of filarial nematodes, includ-

ing the hypodermis and reproductive tissue of adult parasites (1). In contrast to their relatives in arthropods, *Wolbachia* spp. in filarial nematodes appear to have evolved as an essential endosymbiont. Antibiotic therapy in humans and experimental filarial infection has shown that embryogenesis is completely dependent on the presence of

Wolbachia (2, 3). Furthermore, parasites recovered from tetracycline-treated animals are stunted, and larval development is attenuated (2). In *O. volvulus*-infected individuals, adult worms survive for up to 14 years in subcutaneous nodules in the human host and release millions of microfilariae over this time (4). Microfilariae migrate through the skin and can enter the posterior and anterior regions of the eye. While alive, the microfilariae appear to cause little or no inflammation; however, when they die, either by natural attrition or after chemotherapy, the host response to degenerating worms can result in ocular inflammation that causes progressive loss of vision and ultimately leads to blindness (4, 5).

Following the discovery of endosymbiont-derived endotoxin-like activity of *B. malayi* and *O. volvulus* (6, 7), we sought to determine the role of *Wolbachia* in the

¹Division of Geographic Medicine, ²Department of Ophthalmology, University Hospitals of Cleveland and Case Western Reserve University, Cleveland, OH 44106, USA. ³Bernhard Nocht Institute for Tropical Medicine, 20359 Hamburg, Germany. ⁴Liverpool School of Tropical Medicine, Pembroke Place, Liverpool L3 5QA, UK.

*To whom correspondence should be addressed. E-mail: exp2@po.cwru.edu

pathogenesis of ocular onchocerciasis. We used a murine model of corneal inflammation (keratitis) in which parasite extracts were injected directly into the corneal stroma, and corneas were examined by scanning confocal microscopy using confocal microscopy through focusing software (CMTF), (8, 9). This method measures stromal thickness and stromal haze, which are indicators of corneal edema and opacity, respectively, and can measure corneal inflammatory responses that cannot be detected by slit lamp microscopy. To determine the role of *Wolbachia* in *O. volvulus* keratitis, we compared soluble extracts of worms recovered from doxycycline-treated individuals with worms from untreated individuals (3). The effect of doxycycline on reducing *Wolbachia* numbers in the worms was demonstrated by immunohistochemistry with antibodies to bacterial heat shock protein 60 (hsp60) (3). Furthermore, semi-quantitative polymerase chain reaction with *Wolbachia* 16S ribosomal DNA and filarial 5S DNA showed that the 16S/5S index in doxycycline-treated worms was lower than that in untreated worms by a factor of 32 (10).

Extracts from doxycycline-treated worms induced significantly lower stromal thickness, stromal haze, and neutrophil infiltration than extracts from untreated worms (Fig. 1A). Although minor compared with untreated worms, extracts from treated worms also induced inflammatory responses that were significantly higher than those from naïve corneas or corneas injected with saline. Similarly, extracts from the rodent filaria *Acanthocheilonema viteae*, which do not harbor *Wolbachia* (1), induced significantly less stromal thick-

ness, stromal haze, and neutrophil infiltration than extracts from *Brugia malayi* (Fig. 1B). Together, these data indicate that endosymbiotic *Wolbachia* bacteria in filarial parasites have a major role in the development of corneal pathology.

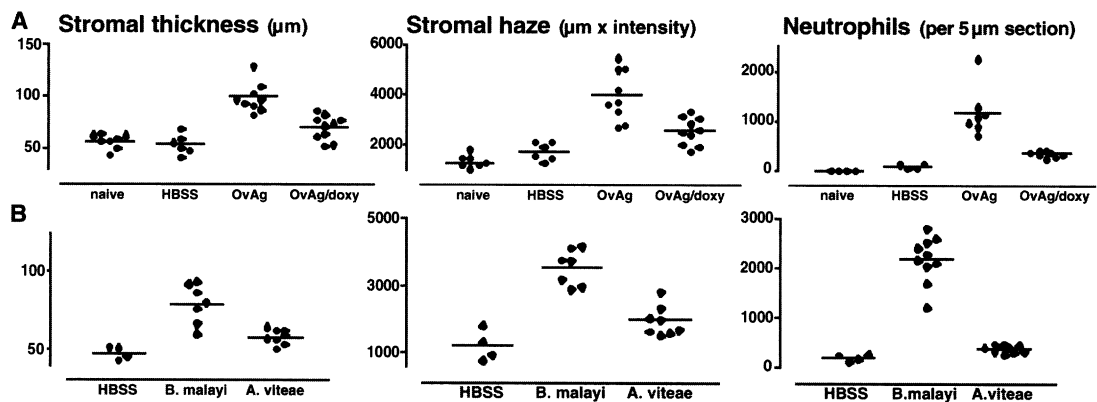
Because TLR4 is essential for the host cell response to bacterial lipopolysaccharide (LPS) (11, 12), we determined if *Wolbachia* mediate corneal pathology by activating TLR4. *O. volvulus* extracts (containing *Wolbachia*) were injected into corneas of C3H/HeJ mice, which are hyporesponsive to LPS owing to a single point mutation in the *Tlr4* gene (13), and immune responses to these extracts were compared with those from congenic, LPS-responsive C3H/HeN mice. Stromal thickness, stromal haze, and neutrophil recruitment were significantly diminished in C3H/HeJ mice compared with C3H/HeN mice (Fig. 2A), indicating that TLR4 regulates the development of *O. volvulus* keratitis. Expression of platelet endothelial cell adhesion molecule-1 (PECAM-1), macrophage inflammatory protein-2 (MIP-2), and KC, which are essential for neutrophil recruitment to the cornea (14, 15), was significantly diminished in C3H/HeJ mice compared with C3H/HeN mice (Fig. 2B), indicating that TLR4 regulates *O. volvulus* keratitis by modulating expression of PECAM-1, MIP-2, and KC in the cornea.

Previous studies showed an important role for T cells, parasite-specific antibodies, and formation of immune complexes in *O. volvulus* keratitis (16, 17). Here, we sought to determine whether TLR4 also regulates keratitis in the presence of an adaptive immune response. C3H/HeN and C3H/HeJ mice were immunized subcutane-

ously and injected intrastromally with a soluble extract from untreated *O. volvulus* worms (containing *Wolbachia*) (18, 19). Stromal thickness, stromal haze, and neutrophil infiltration were assessed at 24 and 72 hours, and eosinophil infiltration was examined after 72 hours, when there is a pronounced eosinophil infiltration in immunocompetent mice (14, 16). C3H/HeJ mice had significantly less stromal thickness, stromal haze, and neutrophils than C3H/HeN mice (Fig. 3, A and B). However, there was no significant difference in eosinophils between C3H/HeJ and C3H/HeN mice at 72 hours (Fig. 3C), indicating that in contrast to neutrophils, eosinophil recruitment to the corneal stroma is not regulated by TLR4.

When taken together, these findings demonstrate an essential role for *Wolbachia* and TLR4 in corneal pathology, even in the presence of an adaptive immune response. These results also indicate that the innate immune system plays a critical role in the inflammatory response associated with the pathogenesis of river blindness. In infected individuals, the innate inflammatory response is therefore likely to be initiated by release of *Wolbachia* endotoxin-like molecules from dead and degenerating worms, which then activate TLR4 on resident corneal epithelial cells and keratocytes. Because corneal cells express functional CD14 and TLR4 that mediate endotoxin-induced interleukin-6 (IL-6) and IL-8 production (20), it is likely that TLR4 activation results in production of chemotactic cytokines in the corneal stroma and PECAM-1 expression on limbal vessels, which facilitate recruitment of neutrophils to the corneal stroma, neutrophil activation,

Fig. 1. (A) *O. volvulus* worms containing *Wolbachia* were recovered from infected individuals in Ghana who were either untreated (OvAg) or had been treated with doxycycline (OvAg/doxy) (3). Soluble extracts were prepared from these worms as described (6), and 1 µg was injected into the corneal stroma of C57Bl/6 mice. Stromal thickness and haze were measured by CMTF (8, 9), and the number of neutrophils per 5-µm corneal section was determined after immunostaining (14, 27). For controls, corneas were either untreated (naïve) or were injected with Hanks' balanced salt solution (HBSS). Data points represent individual corneas from a single experiment. Significant differences were found for all parameters between extracts from doxycycline-treated and from untreated worms ($P < 0.0001$), and between doxycycline-treated and HBSS-treated worms ($P < 0.05$). (B) *B. malayi* and *A. viteae* worms were recovered from gerbils, and soluble extracts were prepared as de-



scribed (7). Parasite extract (1 µg) was injected into C57Bl/6 mice, and stromal thickness, stromal haze, and neutrophil infiltration were determined as described in (A). Data points represent individual corneas from a single, representative experiment. $P < 0.0001$ for *B. malayi* versus *A. viteae* for all parameters, and $P < 0.05$ for *A. viteae* versus HBSS for all parameters. All experiments were repeated at least three times with similar results.

and subsequent loss of corneal function.

Although the role of *Wolbachia* and eosinophils has yet to be determined in chronic infection, and further studies are needed to determine the basis for the *Wolbachia* and TLR4-independent responses, several observations support an important role for *Wolbachia* and the innate response in individuals infected with filarial nematodes. First, fewer neutrophils are detected in nod-

ules of doxycycline-treated individuals compared with untreated individuals (21), indicating that *Wolbachia* mediate neutrophil recruitment in human onchocerciasis. Second, local diethylcarbamazine (DEC) application to the skin of infected individuals causes abscess formation that is associated with an intense neutrophil infiltrate compared with infiltration by eosinophils (22). Third, in human lymphatic filariasis,

release of *Wolbachia* into the blood following anti-filarial drug treatment coincides with the onset of severe systemic inflammation (23).

Wolbachia have emerged as the only target for a chemotherapy that results in long-term sterility of the worms in human onchocerciasis (24, 25), a priority research objective for the World Health Organization for the last 20 years (26). *Wolbachia* depletion by effective treatment with antibiotics such as doxycycline leads to reduction of microfilariae in the skin and to a drastic improvement of skin lesions in hyperergic onchocerciasis (sowda) (24, 25). The results presented here demonstrate that in addition to targeting *Wolbachia* for sustained anti-filarial effects, clearance of *Wolbachia* by antibiotic treatment may also reduce and prevent ocular onchocerciasis.

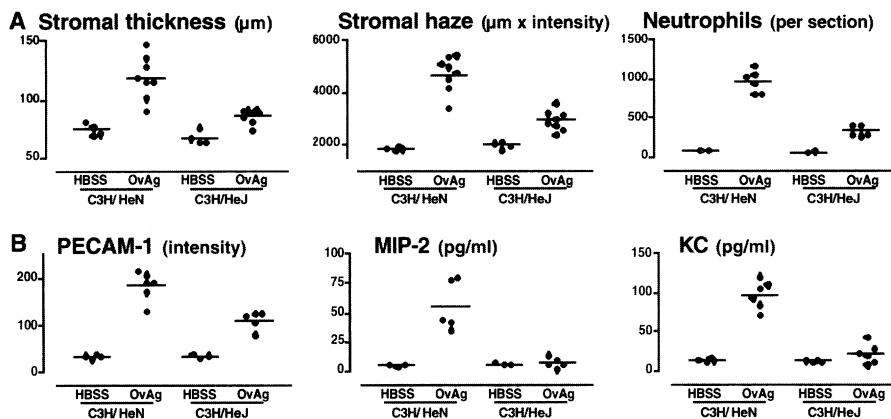


Fig. 2. (A) *O. volvulus* extract (containing *Wolbachia*) was injected into corneas of LPS-hyporesponsive C3H/HeJ mice or congenic C3H/HeN mice. Stromal thickness, haze, and neutrophil numbers were determined as described in Fig. 1. Data points represent individual corneas from a representative experiment. $P < 0.0001$ for C3H/HeJ versus C3H/HeN mice for all parameters measured. (B) C3H/HeJ and C3H/HeN mice were injected intrastromally with *O. volvulus* extracts containing *Wolbachia* bacteria, and PECAM-1 expression on limbal vessels and MIP-2 and KC production were determined as described (27, 28). Data points represent individual corneas from a representative experiment. $P < 0.0001$ for C3H/HeN versus C3H/HeJ mice for PECAM-1, MIP-2, and KC.

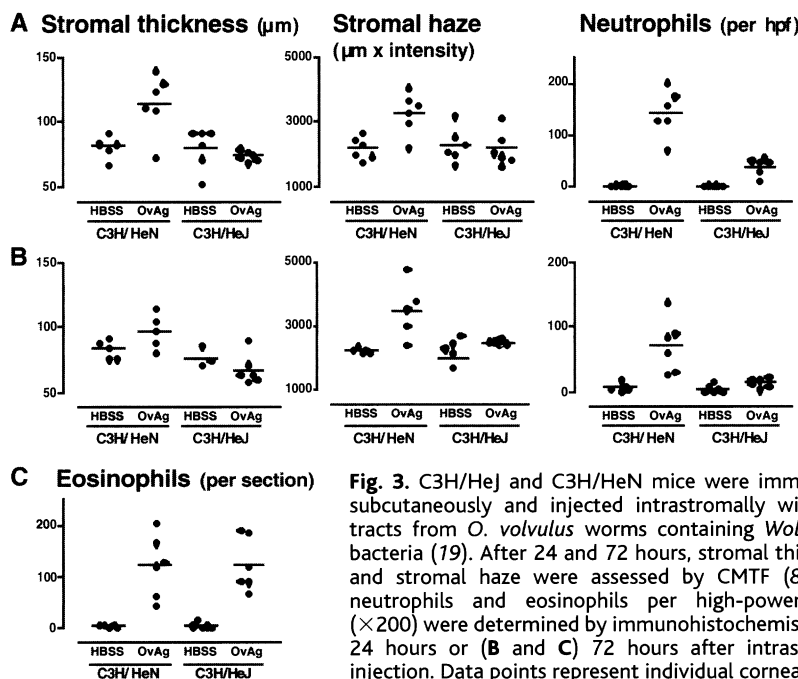


Fig. 3. C3H/HeJ and C3H/HeN mice were immunized subcutaneously and injected intrastromally with extracts from *O. volvulus* worms containing *Wolbachia* bacteria (19). After 24 and 72 hours, stromal thickness and stromal haze were assessed by CMTF (8), and neutrophils and eosinophils per high-power field ($\times 200$) were determined by immunohistochemistry (A) 24 hours or (B and C) 72 hours after intrastromal injection. Data points represent individual corneas from a single experiment. $P < 0.05$ for immunized C3H/

HeN versus C3H/HeJ mice for neutrophils, stromal thickness, and stromal haze at both time points. There was no significant difference in eosinophil numbers between C3H/HeN versus C3H/HeJ mice.

References and Notes

1. M. J. Taylor, A. Hoerauf, *Parasitol. Today* **15**, 437 (1999).
2. A. Hoerauf et al., *J. Clin. Invest.* **103**, 11 (1999).
3. A. Hoerauf et al., *Lancet* **355**, 1242 (2000).
4. www.who.int/ocp/apoc/apoc002.htm (2002).
5. L. R. Hall, E. Pearlman, *Clin. Microbiol. Rev.* **12**, 445 (1999).
6. N. W. Brattig et al., *Microbes Infect.* **2**, 1147 (2000).
7. M. J. Taylor, H. F. Cross, K. Biló, *J. Exp. Med.* **191**, 1429 (2000).
8. Corneas were examined in vivo by scanning confocal microscopy, and stromal thickness and haze values were calculated from intensity profiles generated by CMTF, at 60 frames/s, a lens speed of 160 mm/s, and constant gain.
9. J. Li, J. V. Jester, H. D. Cavanagh, T. D. Black, W. M. Petroll, *Invest. Ophthalmol. Vis. Sci.* **41**, 2945 (2000).
10. A. v. Saint André et al., data not shown.
11. J. C. Chow, D. W. Young, D. T. Golenbock, W. J. Christ, F. Gusovsky, *J. Biol. Chem.* **274**, 10689 (1999).
12. K. Hoshino et al., *J. Immunol.* **162**, 3749 (1999).
13. A. Poltorak et al., *Science* **282**, 2085 (1998).
14. J. T. Kaifi, E. Diaconu, E. Pearlman, *J. Immunol.* **166**, 6795 (2001).
15. L. R. Hall, E. Diaconu, R. Patel, E. Pearlman, *J. Immunol.* **166**, 4035 (2001).
16. L. R. Hall, E. Diaconu, E. Pearlman, *J. Immunol.* **167**, 919 (2001).
17. L. R. Hall, J. H. Lass, E. Diaconu, E. R. Strine, E. Pearlman, *J. Immunol.* **163**, 4970 (1999).
18. E. Pearlman et al., *J. Exp. Med.* **182**, 931 (1995).
19. Corneas were abraded by using a 30-gauge needle, and 1 μ g of extract in 5 μ l of saline was injected directly into the corneal stroma. Preliminary studies indicated that this was the optimal protein concentration for CMTF analysis, and that 24 hours after injection was the optimal time point to examine unimmunized mice. For Fig. 3, animals were immunized subcutaneously with 3 weekly injections of 10 μ g of extract in squalene adjuvant, as described (17).
20. P. I. Song et al., *Invest. Ophthalmol. Vis. Sci.* **42**, 2867 (2001).
21. N. W. Brattig, D. W. Buttner, A. Hoerauf, *Microbes Infect.* **3**, 439 (2001).
22. E. J. Gutierrez-Pena, J. Knab, D. W. Buttner, *Parasitology* **113**, 403 (1996).
23. H. F. Cross, M. Haarbrink, G. Egerton, M. Yazdanbakhsh, M. J. Taylor, *Lancet* **358**, 1873 (2001).
24. A. Hoerauf, S. Mand, O. Adjei, B. Fleischer, D. W. Buttner, *Lancet* **357**, 1415 (2001).
25. M. J. Taylor, A. Hoerauf, *Curr. Opin. Infect. Dis.* **14**, 727 (2001).

26. *Onchocerciasis and Its Control*, vol. 852 (World Health Organization, Geneva, 1995).
27. For immunohistochemistry, eyes were enucleated and snap frozen in liquid nitrogen. Sections (5 μm) were fixed in 4% formaldehyde for 25 min and incubated with rat antibodies to mouse neutrophil (NIMP R14, provided by T. Bianco, Liverpool School of Tropical Medicine; final concentration, 8 mg/ml), rabbit anti-eosinophil major basic protein (1:5000, provided by J. Lee, Mayo Clinic, Scottsdale, AZ), or anti-PECAM-1 (MEC13.3; BD-Pharmingen, CA). Sections were then incubated with fluorescein isothiocyanate-conjugated anti-rat or anti-rabbit im-

- munoglobulin G (Vector Laboratories, Burlingame, CA) and examined by fluorescent microscopy. Cells were counted either throughout the corneal section or in representative 200 \times fields. Images of limbal vessels were captured with a Scion digital camera apparatus (Olympus), and PECAM-1 expression was determined by image analysis (Adobe Photoshop).
28. For KC and MIP-2 ELISAs, corneas were dissected, suspended in 400 ml of RPMI 1640 medium, and sonicated for 90 s at 50 cycles/s (Sonic VibraCell, Danbury, CT). After centrifugation, the concentration of cytokines in supernatants was determined by two-

site enzyme-linked immunosorbent assay (R&D Systems, Minneapolis, MN).

29. Supported by the National Institutes of Health grants EY10320 (E.P.) and EY11373 (J.H.L.), German National Merit Foundation, Studienstiftung des deutschen Volkes (A.v.S.A.), European Union INCO-DEV grant ICA4-CT-1999-10002 (A.H.), German Research Foundation (Deutsche Forschungsgemeinschaft) grant Ho2009/1-3 (A.H.), Wellcome Trust grant 047176 (M.J.T.), Fight for Sight (N.M.B.), and Research to Prevent Blindness Foundation (J.H.L.).

6 December 2001; accepted 5 February 2002

Regulation of Corepressor Function by Nuclear NADH

Qinghong Zhang,¹ David W. Piston,² Richard H. Goodman^{1*}

The corepressor CtBP (carboxyl-terminal binding protein) is involved in transcriptional pathways important for development, cell cycle regulation, and transformation. We demonstrate that CtBP binding to cellular and viral transcriptional repressors is regulated by the nicotinamide adenine dinucleotides NAD⁺ and NADH, with NADH being two to three orders of magnitude more effective. Levels of free nuclear nicotinamide adenine dinucleotides, determined using two-photon microscopy, correspond to the levels required for half-maximal CtBP binding and are considerably lower than those previously reported. Agents capable of increasing NADH levels stimulate CtBP binding to its partners in vivo and potentiate CtBP-mediated repression. We propose that this ability to detect changes in nuclear NAD⁺/NADH ratio allows CtBP to serve as a redox sensor for transcription.

CtBP was initially identified through its ability to interact with the COOH-terminus of adenovirus E1A. Mutation of the CtBP binding site in E1A decreases its transcriptional repression effects and increases its ability to direct cellular transformation (1, 2). CtBP also participates in the actions of cellular transcription factors involved in growth and differentiation, as demonstrated in *Drosophila melanogaster* (3) and vertebrate systems (4). The recent demonstration that yeast Sir2 utilizes NAD⁺ as a substrate (5–7) and the remarkable sequence conservation of CtBP with the dehydrogenases and reductases (2) (Fig. 1A), enzymes that use nicotinamide adenine dinucleotides as cofactors, led us to investigate whether CtBP might similarly be regulated by NAD⁺ or NADH.

CtBP expressed in bacteria or isolated from HeLa cells was incubated with glycerophosphate, acetoacetate, pyruvate, lactate, acetate, formate, and ethanol in the presence of NAD⁺ or NADH under a variety of experimental conditions. No dehy-

drogenase or reductase activity was detected. We next tested whether CtBP was regulated in some other manner by NAD⁺ or NADH. This hypothesis was suggested by the near-perfect conservation of the NAD⁺/NADH binding signature near the middle of the CtBP sequence (Fig. 1B). One possibility was that NAD⁺/NADH could affect the ability of CtBP to interact with its partners. To test this hypothesis, we examined the interaction of bacterially expressed CtBP with glutathione S-transferase (GST)-E1A fusion proteins at different concentrations of NAD⁺/NADH. To our surprise, CtBP binding was regulated dramatically, with NADH increasing the interaction at concentrations in the nM range (Fig. 1C). NAD⁺ also increased binding, but was 2 to 3 orders of magnitude less effective. NADP⁺, NADPH, and flavin adenine dinucleotide (FAD⁺) had little effect (Fig. 1D) (8). NAD⁺/NADH similarly affected CtBP binding to a prototypical cellular repressor, ZEB (Fig. 1E), which is known to block transcription at least in part via CtBP interactions (9).

Knowing the physiological concentrations of free nuclear NAD⁺/NADH is critical for assessing whether these molecules regulate CtBP function in vivo, the concentration of NAD(P)H can be determined in different cellular compartments using two-photon excitation microscopy (10). This

was done in Cos7 cells by quantitative imaging of the total intensity and lifetime of NAD(P)H fluorescence. For these measurements, NADH and NADPH are indistinguishable, so we measure the sum of both molecules. Comparing the total intensity to a standard curve of free NAD(P)H in solution, we found that the nucleus contained 113 μM NAD(P)H (Fig. 2A). Precise determination of the concentration is complicated by the fact that the fluorescence of free and bound forms of NAD(P)H differs. Free NAD(P)H has a considerably lower quantum efficiency than that bound to protein. Because the quantum efficiency is associated with the fluorescence lifetime, we can determine the fraction of bound NAD(P)H by fluorescence lifetime imaging (11). The fluorescence lifetime image was homogeneous across all subcellular compartments (Fig. 2B) with a value of 3.41 ns ($n = 6$ cells), as compared to 0.45 ns for free NAD(P)H. This indicates that the vast majority of NAD(P)H is bound and that our estimate of 113 μM is ~ 7.5 -fold too high (ratio of 3.41 to 0.45). The corrected nuclear NAD(P)H concentration is thus ~ 15 μM . To quantitate the amount of free NAD(P)H, we performed a multifrequency experiment with phase modulations at 80, 160, and 240 MHz and fit multiple exponential decays to the fluorescence lifetimes. One lifetime component was fixed at 0.451 ns [the lifetime for free NAD(P)H], and the other was allowed to vary with the nonlinear least squares fit. According to this fit, the fraction of fluorescence associated with the free component was $4.4 \pm 2.7\%$. Thus, the upper limit of free NAD(P)H is 660 nM. If we assume that the NADPH/NADH ratio is ~ 4 (12), then the concentration of free NADH in the nucleus is ~ 130 nM (13), well within the range required for stimulating the E1A:CtBP interaction.

Because NAD⁺/NADH affected CtBP binding to multiple transcriptional repressors, we speculated that these cofactors most likely functioned by altering CtBP structure. Support for this idea was obtained from limited proteolysis experiments. In the absence of NAD⁺/NADH, trypsin treatment releases a 10-kD fragment from the CtBP NH₂-terminus, resulting in

¹Vollum Institute, Oregon Health Sciences University, 3181 SW Sam Jackson Park Road, Portland, OR 97201, USA.

²Department of Molecular Physiology and Biophysics, Vanderbilt University, 702 Light Hall, Nashville, TN 37232, USA.

*To whom correspondence should be addressed. E-mail: goodmanr@ohsu.edu